radiate during favorable times (*22*). This probably includes the reoccupation of FAY-NE1 during MIS 3 by the population that produced assemblage A. Access from southeast Arabia to the Persian Gulf and vice versa is likely to have been via the numerous wadi channels that extend from the Hajar Mountains and into the Persian Gulf basin, passing Jebel Faya to the north and the south. These channels would also have facilitated human migration by providing access to fresh water along the shores of the proto-Gulf (*22*, *27*).

References and Notes

1. M. D. Petraglia *et al.*, *Science* **317**, 114 (2007).
2. I. McDougall, F. H. Brown, J. G. Fleagle, *Nature* **433**, 733 (2005).
3. M. D. Petraglia, J. I. Rose, Eds. *Evolution of Human Populations in Arabia: Paleoenvironments, Prehistory and Genetics* (Springer, Dordrecht, Netherlands, 2009), pp. 1–14.
4. R. Derricourt, *J. World Prehist.* **19**, 119 (2005).
5. J. J. Shea, *Quat. Sci. Rev.* **27**, 2253 (2008).
6. R. Klein, *Evol. Anthropol.* **9**, 17 (2000).
7. P. Mellars, *Proc. Natl. Acad. Sci. U.S.A.* **103**, 9381 (2006).
8. C. B. Stringer, *Nature* **405**, 24 (2000).
9. D. E. Wildman *et al.*, *Mol. Phylogenet. Evol.* **32**, 287 (2004).
10. L. O. Quintana-Murci *et al.*, *Nat. Genet.* **23**, 437 (1999).
11. T. Kivisild *et al.*, *Am. J. Hum. Genet.* **75**, 752 (2004).
12. P. Forster, S. Matsumura, *Science* **308**, 965 (2005).
13. H. Field, *Am. J. Archaeol.* **36**, 426 (1932).
14. Materials and methods are available as supporting material on *Science* Online.
15. Z. Jacobs, R. R. Roberts, *Evol. Anthropol.* **16**, 210 (2007).
16. A. Marks, in *Evolution of Human Populations in Arabia: Paleoenvironments, Prehistory and Genetics*, M. D. Petraglia, J. I. Rose, Eds. (Springer, Dordrecht, Netherlands, 2009), pp. 295–308.
17. H.-P. Uerpmann, D. T. Potts, M. Uerpmann, in *Evolution of Human Populations in Arabia: Paleoenvironments, Prehistory and Genetics*, M. D. Petraglia, J. I. Rose, Eds. (Springer, Dordrecht, Netherlands, 2009), pp. 205–214.
18. S. McBrearty, *World Archaeol.* **19**, 388 (1988).
19. A. G. Parker, in *Evolution of Human Populations in Arabia: Paleoenvironments, Prehistory and Genetics*, M. D. Petraglia, J. I. Rose, Eds. (Springer, Dordrecht, Netherlands, 2009), pp. 38–49.
20. G. N. Bailey *et al.*, *Coast. Arch* **2**, 127 (2007).
21. M. Siddall *et al.*, *Nature* **423**, 853 (2003).
22. J. I. Rose, *Proc. Semin. Arabian Stud.* **37**, 219 (2007).
23. M. Sarnthein, *Mar. Geol.* **12**, 245 (1972).
24. K. Lambeck, *Earth Planet. Sci. Lett.* **142**, 43 (1996).
25. H.-P. Uerpmann, *The Ancient Distribution of Ungulate Mammals in the Middle East - Fauna and Archaeological Sites in Southwest Asia and Northeast Africa*, Beihefte zum Tübinger Atlas des Vorderen Orients, Reihe A (Naturwissenschaften), Band 27 (Ludwig Reichert Verlag, Wiesbaden, Germany, 1987).
26. C. Becker, *Munibe* **57**, 445 (2005).
27. H. Faure *et al.*, *Global Planet. Change* **33**, 47 (2002).
28. F. Preusser, *C. R. Geosci.* **341**, 621 (2009).
29. S. J. Burns, D. Fleitmann, A. Matter, U. Neff, A. Mangini, *Geology* **29**, 623 (2001).
30. D. Fleitmann, A. Matter, *C. R. Geosci.* **341**, 633 (2009).
31. N. Petit-Maire *et al.*, *Global Planet. Change* **72**, 368 (2010).
32. D. C. Leuschner, F. Sirocko, *Palaeogeogr. Palaeoclimatol. Palaeoecol.* **197**, 83 (2003).
33. M. Bar-Matthews, A. Ayalon, M. Gilmour, A. Matthews, C. J. Hawkesworth, *Geochim. Cosmochim. Acta* **67**, 3181 (2003).
34. D. G. Martinson *et al.*, *Quat. Res.* **27**, 1 (1987).

35. Funding information: We thank the government of Sharjah for funding the excavations and elements of the lab work at Tübingen. Funding was also provided by the Role of Culture in Early Expansions of Humans project (Heidelberg Academy of Sciences), Humboldt Foundation, Oxford Brookes University, and the German Science Foundation (Deutsche Forschungsgemeinschaft). Author responsibilities: S.J.A., OSL dating; S.A.J., excavation codirector; A.E.M. and V.I.U., lithic analysis; A.G.P., paleoenvironments; H.-P.U., codirector of excavations, director of laboratory analyses at Tübingen University. Special thanks are due to the third codirector, M. Uerpmann, for handling the logistics of the project.

Supporting Online Material

www.sciencemag.org/cgi/content/full/331/6016/453/DC1
Materials and Methods
SOM Text
Figs. S1 to S10
Tables S1 to S8
References and Notes

15 October 2010; accepted 28 December 2010
10.1126/science.1199113

Phosphorylation of ULK1 (hATG1) by AMP-Activated Protein Kinase Connects Energy Sensing to Mitophagy

Daniel F. Egan,[1] David B. Shackelford,[1] Maria M. Mihaylova,[1,2] Sara Gelino,[4] Rebecca A. Kohnz,[1] William Mair,[1] Debbie S. Vasquez,[1] Aashish Joshi,[5] Dana M. Gwinn,[1] Rebecca Taylor,[1] John M. Asara,[6] James Fitzpatrick,[3] Andrew Dillin,[1,2] Benoit Viollet,[7] Mondira Kundu,[5] Malene Hansen,[4] Reuben J. Shaw[1,2]*

Adenosine monophosphate–activated protein kinase (AMPK) is a conserved sensor of intracellular energy activated in response to low nutrient availability and environmental stress. In a screen for conserved substrates of AMPK, we identified ULK1 and ULK2, mammalian orthologs of the yeast protein kinase Atg1, which is required for autophagy. Genetic analysis of AMPK or ULK1 in mammalian liver and *Caenorhabditis elegans* revealed a requirement for these kinases in autophagy. In mammals, loss of AMPK or ULK1 resulted in aberrant accumulation of the autophagy adaptor p62 and defective mitophagy. Reconstitution of ULK1-deficient cells with a mutant ULK1 that cannot be phosphorylated by AMPK revealed that such phosphorylation is required for mitochondrial homeostasis and cell survival during starvation. These findings uncover a conserved biochemical mechanism coupling nutrient status with autophagy and cell survival.

A highly conserved sensor of cellular nutrient status found in all eukaryotes is the adenosine monophosphate (AMP)–activated protein kinase (AMPK). In response to decreases in intracellular ATP, AMPK is activated and serves as a metabolic checkpoint, restoring ATP levels through acute regulation of metabolic enzymes and inhibition of pro-growth anabolic pathways (*1*). Inactivation of LKB1, the upstream kinase necessary for activation of AMPK under low-energy conditions, is a frequent event in several forms of human cancer (*2*). In addition, LKB1 signaling is required in the liver for the therapeutic effect of metformin, the most prevalent type 2 diabetes drug worldwide, and LKB1 inactivation in mouse liver results in a type 2 diabetes–like metabolic disease (*3*). Thus the LKB1-AMPK pathway provides a direct link between tumor suppression and control of cellular and organismal metabolism.

Similar to AMPK activation, the cellular process of autophagy is initiated under nutrient-poor and low-energy conditions as a survival mechanism to ensure availability of critical metabolic intermediates and to eliminate damaged organelles, including mitochondria (*4*). Autophagy is thought to be initiated under nutrient-limited conditions by a conserved kinase complex containing the serine-threonine kinase Atg1 and its associated subunits, Atg13 and Atg17 (*5*). In mammals, this complex is encoded by two Atg1 homologs, ULK1 and ULK2, and the subunits Atg13 and FIP200, which signal to downstream autophagy regulators through still poorly understood mechanisms. In yeast and mammalian cells, Atg1 or ULK1 activity is suppressed under nutrient-rich conditions by the TOR (target of rapamycin) complex 1 (TORC1) (*6*). However, biochemical events that activate Atg1 or ULK1 have not yet been identified.

We used a two-part screen to identify substrates of AMPK that mediate its effects on cell

[1]Molecular and Cell Biology Laboratory, Dulbecco Center for Cancer Research, Salk Institute for Biological Studies, La Jolla, CA 92037, USA. [2]Howard Hughes Medical Institute, Salk Institute for Biological Studies, La Jolla, CA 92037, USA. [3]Waitt Advanced Biophotonics Center, Salk Institute for Biological Studies, La Jolla, CA 92037, USA. [4]Graduate School of Biomedical Sciences, Del E. Webb Neuroscience, Aging and Stem Cell Research Center, Sanford-Burnham Medical Research Institute, La Jolla, CA 92037, USA. [5]Department of Pathology, St. Jude Children's Research Hospital, Memphis, TN 38105, USA. [6]Division of Signal Transduction, Beth Israel Deaconess Medical Center, and Department of Medicine, Harvard Medical School, Boston, MA 02115, USA. [7]Inserm, U1016, Institut Cochin, Université Paris Descartes, CNRS (UMR 8104), Paris, France.

*To whom correspondence should be addressed. E-mail: shaw@salk.edu

growth and metabolism (*7*). First, we used an optimal AMPK substrate motif (*8*) to search eukaryotic databases for proteins containing conserved candidate target sites. Many in vivo substrates of AMPK not only conform to this motif but also bind to the phospho-binding protein 14-3-3 inducibly upon phosphorylation by AMPK. We therefore screened for proteins that bound to recombinant 14-3-3 in wild-type (WT) but not AMPK-deficient cells, and only under conditions of energy stress, when AMPK would be active. One protein we identified that contained multiple conserved candidate AMPK phosphorylation sites and associated with 14-3-3 in an AMPK-dependent manner was the mammalian Atg1 homolog ULK1 (Fig. 1, A and B). ULK1 contains four sites (Ser^{467}, Ser^{555}, Thr^{574}, and Ser^{637}) matching the optimal AMPK substrate motif, all of which are conserved in higher eukaryotes. Two of the sites are conserved back to *Caenorhabditis elegans* (Ser^{555} and Ser^{574}) and in the mammalian family member ULK2, though not the more distant family members ULK3 and ULK4, which unlike ULK1 and ULK2 are not thought to function in autophagy. Indeed, endogenous AMPK subunits co-immunoprecipitated with ULK1 and ULK2 but not ULK3 (fig. S1), and AMPK subunits were found in unbiased identifications of proteins co-immunoprecipitating with overexpressed ULK2 (fig. S2), which is consistent with recent proteomic analyses (*9*). To examine ULK1 in vivo phosphorylation sites, we used tandem mass spectrometry on epitope-tagged ULK1 isolated from cells treated with or without the mitochondrial complex I inhibitor phenformin (*10*). We detected peptides spanning three of the four candidate AMPK sites in ULK1 (Ser^{555}, Thr^{574}, and Ser^{637}), and all three were phosphorylated only after phenformin treatment (figs. S3 and S4). To examine whether ULK1 could serve as a direct substrate for AMPK in vitro, we created a kinase-inactive allele (K46I) (*11*) to remove its autophosphorylation. AMPK phosphorylated ULK1 to a greater extent than it did an established substrate, Raptor (Fig. 1C and fig. S5), which may reflect the presence of at least four potential AMPK sites in ULK1, as compared with Raptor, which has two reported AMPK sites (*8*). We gen-

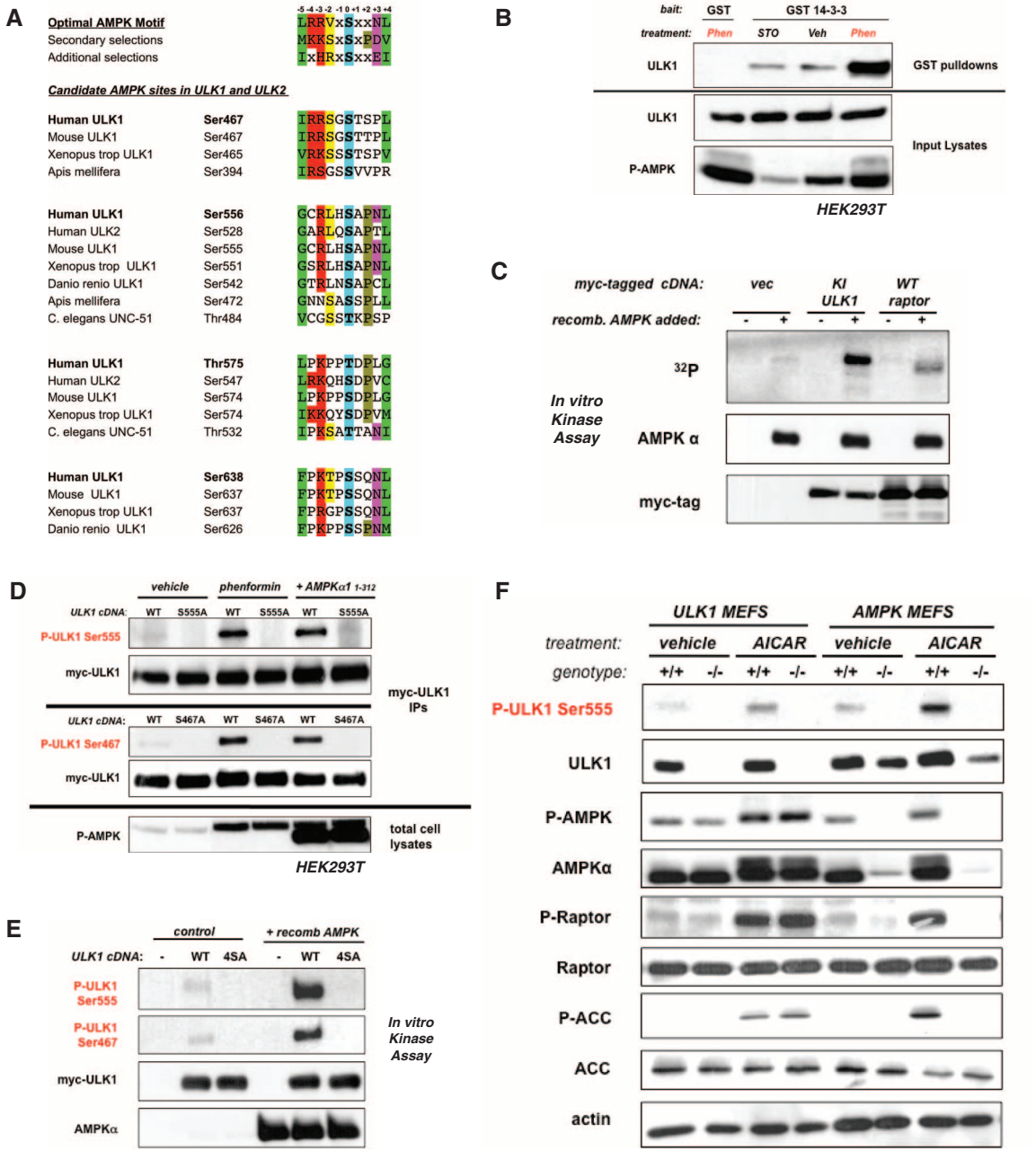

Fig. 1. ULK1 is a conserved substrate of AMPK. (**A**) Clustal alignment of four conserved sites in ULK1 and two sites in ULK2 matching the optimal AMPK substrate motif. (**B**) ULK1 and glutathione *S*-transferase (GST) or GST-14-3-3 expression vectors were transfected into human embryonic kidney (HEK) 293T cells, and placed in media containing 20 μM STO-609 (STO), vehicle (veh), or 5 mM phenformin (Phen) for 1 hour. Cell lysates and GST pulldowns were immunoblotted as indicated. (**C**) In vitro kinase assays with myc-tagged catalytically inactive (KI: K46I) ULK1 or myc-tagged WT raptor that were immunoprecipitated from HEK293T cells and used as substrates for purified active AMPK in the presence of ^{32}P-(C)-ATP. (**D**) HEK293T cells transfected with myc-tagged WT ULK1 or indicated serine-to-alanine ULK1 mutants were treated with either vehicle or 1 mM phenformin for 1 hour or were cotransfected with a constitutively active AMPKα1 (aa1-312) mammalian expression vector (*12*). Proteins from lysates were immunoblotted with phospho-specific antibodies as indicated. (**E**) In vitro kinase assays using myc-ULK1 and purified AMPK as above. Phosphorylation of myc-ULK1 detected through immunoblotting with indicated phospho-specific antibodies. (**F**) Primary MEFs were treated with 2 mM AICAR or vehicle for 1 hour. Lysates were immunoblotted as indicated, including detection of endogenous ULK1 P-Ser^{555}.

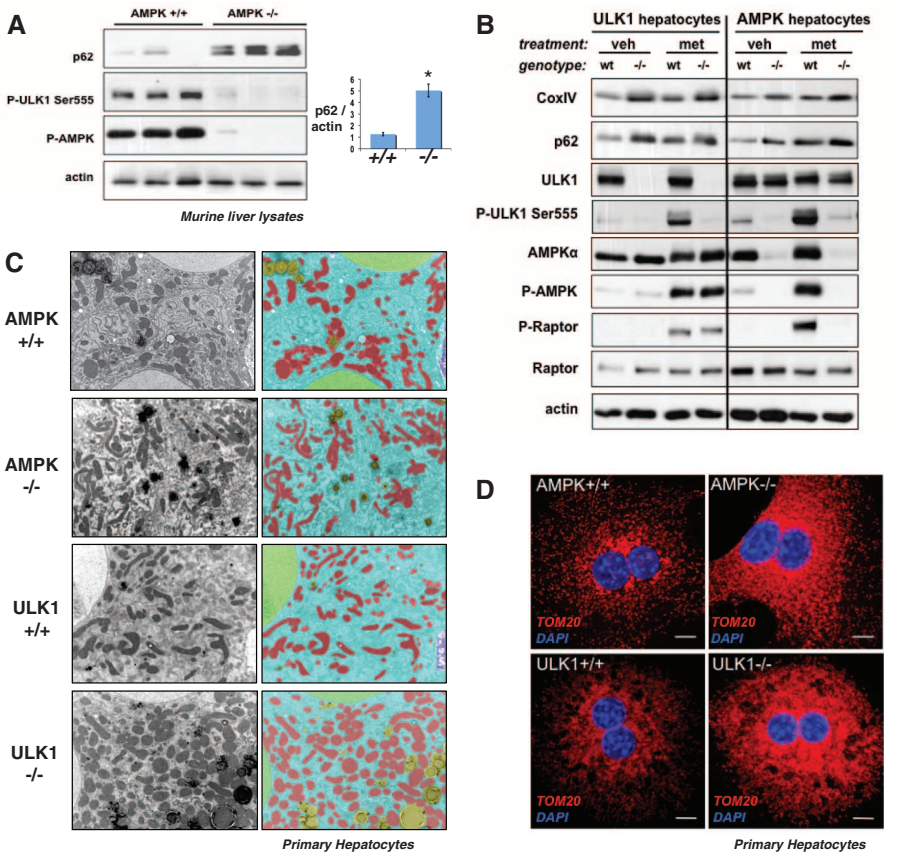

Fig. 2. Genetic deficiency for AMPK or ULK1 in mouse liver or primary mouse hepatocytes results in autophagy defects. (**A**) Liver lysates from littermate-matched mice were immunoblotted for the indicated antibodies. p62-to-actin ratio calculated from densitometry performed on immunoblots. Data shown as mean ± SEM. *$P < 0.01$. (**B**) Primary hepatocytes derived from ULK1$^{+/+}$ or ULK1$^{-/-}$ mice or AMPKa1$^{+/-}$a2$^{L/+}$ or AMPKa1$^{-/-}$a2$^{L/L}$ as described in (*7*) were placed in media containing 2 mM metformin (met) or vehicle (veh) for 2 hours. Lysates were immunoblotted with the indicated antibodies. (**C**) TEM was performed on primary mouse hepatocytes of the indicated genotypes, revealing accumulation of mitochondria in both AMPK- and ULK1-deficient cells. Red, mitochondria; blue, cytoplasm; green, nuclei; yellow, lipid droplets. (**D**) Primary mouse hepatocytes of the indicated genotypes stained by means of immunocytochemistry for the mitochondrial marker TOM20 (red) and nuclei (blue). Scale bar, 10 μm.

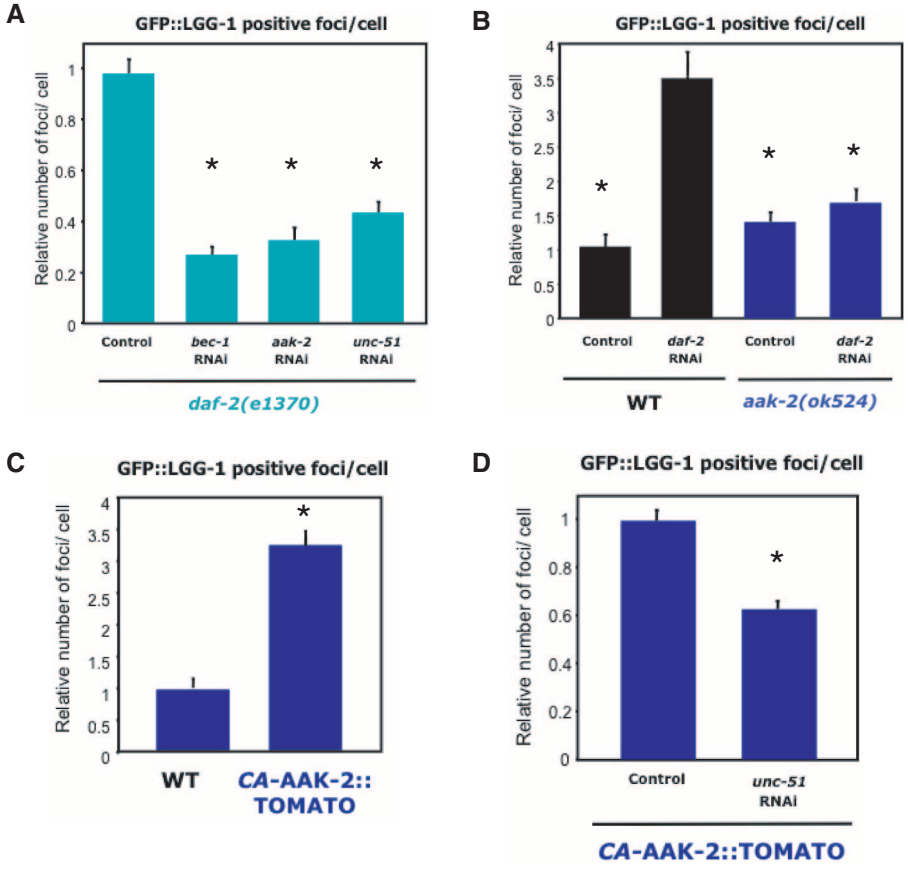

Fig. 3. AMPK is necessary and sufficient for autophagy induction in *C. elegans*. (**A**) Insulin receptor *daf-2(e1370)* mutant worms expressing GFP::LGG-1 (equivalent to GFP-LC3) were treated with control RNAi or RNAi against *bec-1* (Beclin), *aak-2* (AMPKα2), or *unc-51* (ULK1), and the number of LGG-1/LC3–positive puncta per hypodermal seam cell were quantified. (**B**) *aak-2(ok524)* mutants or WT N2 (WT) animals expressing GFP::LGG-1 were treated with control or *daf-2* RNAi and scored for LGG-1 positive puncta per seam cell. (**C**) Transgenic worms expressing constitutively active AAK-2 (*12*) (amino acids 1-321)::TOMATO (CA-AAK-2::TOMATO) fusion or controls (WT) were analyzed for LGG-1–positive puncta per seam cell. (**D**) Animals expressing both CA-AAK-2$_{(1-321)}$::TOMATO and GFP::LGG-1 were treated with control or *unc-51* RNAi and scored for LGG-1/LC3–positive puncta per seam cell. All panels show relative counts; see fig. S10 for details. Data shown as mean ± SEM. *$P < 0.0001$.

erated phosphospecific antibodies against Ser[467] and Ser[555] of ULK1. Phosphorylation of both sites was induced by means of phenformin treatment or expression of ULK1 with a constitutively active AMPKα1 allele (*12*) in the absence of energy stress (Fig. 1D). Purified AMPK also induced phosphorylation at these sites in an in vitro kinase assay, which is consistent with their direct phosphorylation (Fig. 1E). Using AMPK- and ULK1-deficient primary mouse embryonic fibroblasts (MEFs) or matched control WT MEFs, we observed phosphorylation of endogenous ULK1 on Ser[555] in an AMPK-dependent manner after treatment of cells with the AMP-mimetic aminoimidazole carboxamide ribonucleotide (AICAR)

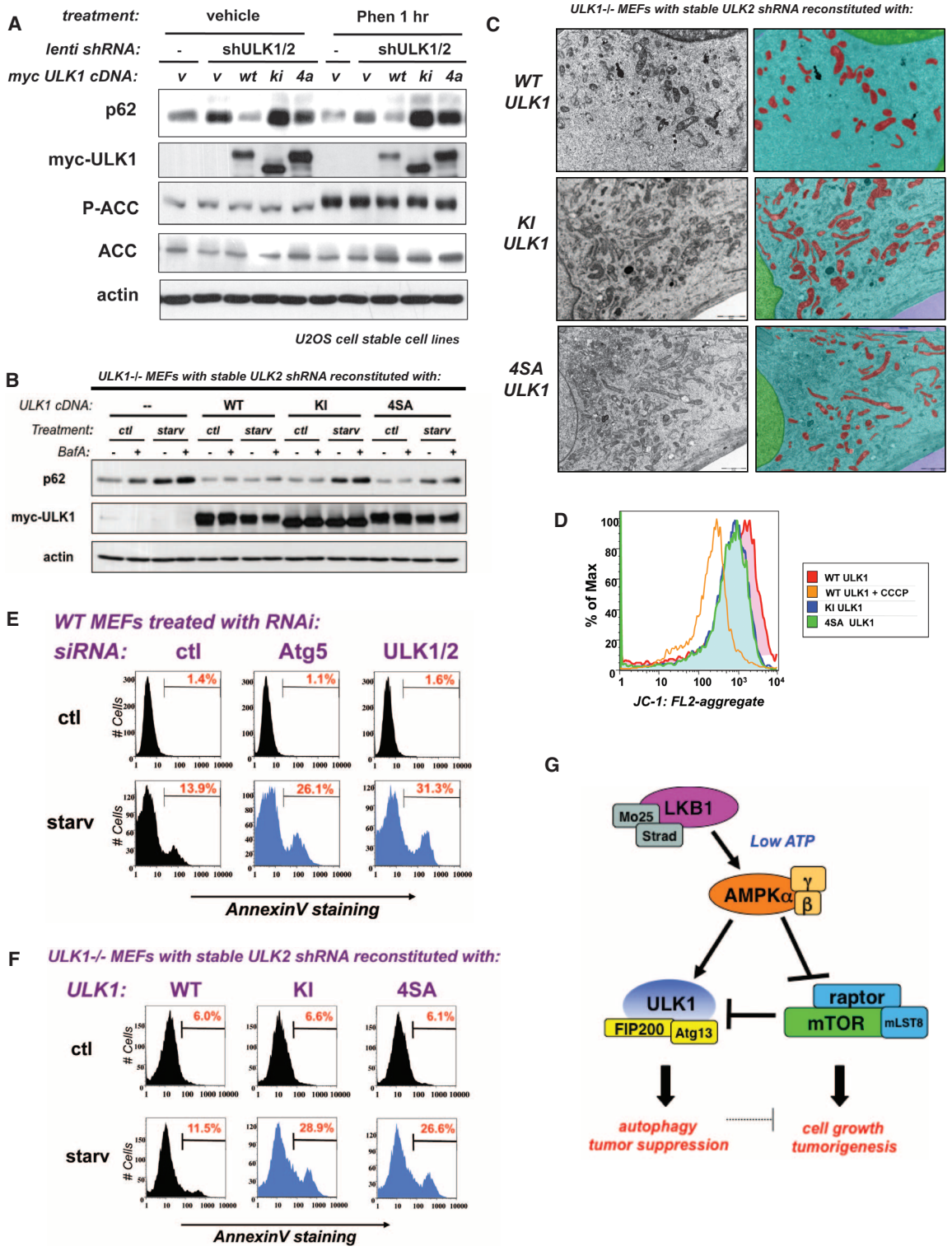

Fig. 4. AMPK phosphorylation of ULK1 is required for mitophagy and cell survival upon nutrient deprivation. (**A**) U2OS cells stably expressing mouse WT, KI, or AMPK 4SA ULK1 cDNA or the empty retroviral vector (v) along with a shRNA against endogenous human ULK1 and ULK2 were placed in media containing 5 mM phenformin (Phen) or vehicle for 1 hour. Lysates were immunoblotted as indicated. (**B**) ULK1$^{-/-}$ MEFs stably expressing WT, KI, or 4SA ULK1 cDNA or the empty retroviral vector (v) along with a shRNA against endogenous ULK2 were placed in Earle's balanced salts solution starvation media (starv) or control media (ctl) for 6 hours in the presence or absence of BafilomycinA (BafA) and immunoblotted as indicated. (**C**) Cells from (B) analyzed with TEM and Inform morphometric software. Red, mitochondria; blue, cytoplasm; green, nuclei. (**D**) Flourescence-activated cell sorting (FACS) analysis on cells from (B), which were stained with JC-1 under basal conditions or with the mitochondrial uncoupler carbonyl cyanide m-chloro phenyl hydrazone (CCCP) as a control in order to measure mitochondrial membrane potential. Compromised mitochondrial membrane potential is shifted to the left, as observed in cells treated with CCCP. (**E**) WT MEFs transfected with 20 nM siRNA pools to a universal control (ctl), mouse Atg5, or mouse ULK1 and ULK2 for 72 hours were then placed in starvation medium (starv) or standard media (ctl) for 12 hours, and cell death was scored by means of AnnexinV-FACS. (**F**) Cells from (B) were placed in starvation medium (starv) or standard media (ctl) for 12 hours, and cell death was scored by means of AnnexinV-FACS. (**G**) Model for AMPK activation of ULK1 in a two-pronged mechanism via direct phosphorylation of ULK1 and inhibition of mTORC1 suppression of ULK1.

(Fig. 1F). The phosphorylation of ULK1 in these cells paralleled that of two bona fide AMPK substrates, acetyl-CoA carboxylase (ACC) and Raptor (Fig. 1F and fig. S6).

We examined the phenotypic consequences of AMPK or ULK1 deficiency on markers of autophagy in mouse liver and primary hepatocytes. Immunoblot and immunohistochemical analysis of AMPK-deficient livers (*13*) showed accumulation of the p62 protein (Fig. 2A and fig. S7), whose selective degradation by autophagy has established it as a widely used marker of this process (*14*). p62 contains a ubiquitin-associated (UBA) ubiquitin-binding domain, which mediates binding to ubiquitinated cargo targeted for autophagy-mediated degradation (*14*). Consistent with this function, p62 aggregates colocalized with ubiquitin aggregates in AMPK-deficient livers (fig. S7). p62 is recruited to mitochondria targeted for mitophagy and is involved in mitochondrial aggregation and clearance (*15*, *16*). ULK1-deficient mice exhibit accumulation of defective mitochondria in mature red blood cells, which are normally devoid of mitochondria (*17*). Given the aberrant accumulation of p62 in the absence of AMPK in mouse liver and the fact that rodent hepatocytes undergo substantial mitophagy upon culturing (*18*), we examined whether AMPK or ULK1 deficiency in primary hepatocytes might exhibit mitochondrial defects. Protein levels of p62 and the mitochondrial marker protein CoxIV were similarly elevated in lysates from AMPK- or ULK1-deficient hepatocytes cells but not from WT controls (Fig. 2B and fig. S8). Increased phosphorylation of endogenous ULK1 Ser^{555} was observed in WT but not AMPK-deficient hepatocytes after AMPK activation by metformin treatment (Fig. 2B). Further analysis of the ULK1 and AMPK hepatocytes by use of transmission electron microscopy (TEM) revealed elevated levels of abnormal mitochondria, which was analyzed quantitatively with morphometric software (Fig. 2C, right). Similar to findings in other autophagy-mutant hepatocytes (*19*), the number of mitochondria per cell was significantly increased in AMPK- and ULK1-deficient hepatocytes as compared with that of WT controls (fig. S9), which is also seen with immunocytochemical staining for the mitochondrial membrane protein TOM20 (Fig. 2D).

Given the conservation of AMPK sites in ULK1, we examined whether these two proteins function together to play conserved roles in autophagy in the nematode *C. elegans*. In a reporter assay based on the *C. elegans* LC3 homolog LGG-1 (*20*, *21*), we observed that loss of insulin signaling through genetic mutation [*daf-2 (e1370)*] or RNA interference (RNAi) against the insulin receptor *daf-2* resulted in increased numbers of green fluorescent protein (GFP):: LGG-1–positive foci in hypodermal seam cells, which is indicative of increased autophagy and consistent with the established role for insulin signaling in the suppression of autophagy in *C. elegans* (*20*–*24*). *daf-2* mutant worms treated with RNAi to *aak-2* or *unc-51*, the AMPK and ULK1 orthologs, respectively, resulted in a decrease in abundance of LGG-1–containing puncta (Fig. 3A). *daf-2* RNAi failed to increase the number of LGG-1–positive foci in AMPK-deficient worms (Fig. 3B). These data indicate that both AMPK and ULK1 have critical roles in autophagy induced by means of reduced insulin signaling in *C. elegans*. Transgenic worms expressing constitutively active AMPK exhibited an approximately threefold increase in the number of LGG-1–positive foci in seam cells as compared with the number of foci in controls (Fig. 3C). The number of LGG-1–positive foci was significantly reduced when these animals were fed unc-51 RNAi (Fig. 3D) (all data can be found in fig. S10). These observations indicate that AMPK activation is sufficient to induce autophagy in worms, and ULK1 is required for this induction.

To test whether AMPK phosphorylation of ULK1 is required for ULK1 function, we stably introduced WT, catalytically inactive (KI), or the AMPK nonphosphorylatable (4SA) ULK1 cDNA into human osteosarcoma U2OS cells in which we subsequently reduced endogenous ULK1 and ULK2 with lentiviral short hairpin RNAs (shRNAs) against each (fig. S11). U2OS cells stably expressing ULK1 and ULK2 shRNA exhibited increased amounts of p62 indicative of defective autophagy as compared with that of parental U2OS cells infected with an empty lentiviral vector (Fig. 4A; compare lane 1 and 2). Stable retroviral reconstitution of a myc-tagged WT ULK1 cDNA, but not the 4SA or KI mutant, restored p62 degradation (Fig. 4A, lanes 3 to 5, and fig. S12). Furthermore, we reconstituted $ULK1^{-/-}$ MEFs that were also knocked down for endogenous ULK2 (fig. S13) with WT, KI, or 4SA ULK1 cDNAs and examined the extent of autophagy after placement of these cell lines into starvation media. MEFs deficient for ULK1 and ULK2 contained elevated levels of p62 upon starvation. Cells reconstituted with WT ULK1 had reduced p62 levels, unlike the KI- or 4SA-expressing cells, which behaved like the ULK-deficient state (Fig. 4B and fig. S14). To test whether the 4SA mutant exhibited effects on mitochondrial homeostasis, we used TEM and mitochondrial-selective dyes on the WT, KI, and 4SA ULK1 stably reconstituted ULK-deficient MEFs. TEM and Mitotracker Red staining revealed that the KI- and 4SA-ULK1–expressing cells had altered mitochondrial homeostasis as compared with that of WT ULK1 cells, denoted by increases in the overall number and aberrant morphology of mitochondria (Fig. 4C and figs. S18 and S19). The altered cristae and aberrant morphology of the mitochondria in the KI- and 4SA-ULK1–reconstituted cells was enhanced upon starvation (fig. S19). To test whether these mitochondria were functionally impaired, we analyzed the mitochondrial membrane potential with the activity-dependent JC-1 dye, which revealed defects in KI- and 4SA-reconstituted MEFs (Fig. 4D).

A hallmark of cells defective for autophagy is a predisposition to undergo apoptosis after stress stimuli that normally would activate autophagy to promote cell survival (*25*). We examined how ULK1/2 deficiency would compare with loss of central downstream autophagic regulator such as Atg5 in terms of requirement for cell survival after starvation. WT MEFs were treated with control, Atg5, or combined ULK1 and ULK2 small interfering RNA (siRNA) and analyzed for effects on cell viability after being placed into starvation conditions. Simultaneous depletion of ULK1 and ULK2 mirrored the magnitude and kinetics of cell death observed with Atg5 loss upon starvation (Fig. 4E and fig. S20). We next investigated whether mutation of the AMPK sites in ULK1 might also mimic ULK1/2 loss of function in this cell survival assay. ULK-deficient MEFs reconstituted with WT, but not KI or 4SA ULK1, restored cell survival upon starvation (Fig. 4F). ULK1-deficient cells expressing the KI or 4SA mutant ULK1 showed rates of cell death similar to those of WT MEFs treated with Ulk1 and Ulk2 siRNA. Thus, loss of the AMPK sites in ULK1 mimics complete loss of ULK1 and ULK2 in control of cell survival after nutrient deprivation.

Our findings reveal a direct connection between energy sensing and core conserved autophagy proteins. In mammals, phosphorylation of ULK1 by AMPK is required for ULK1 function in the response to nutrient deprivation. Because AMPK suppresses mammalian TOR (mTOR) activity and mTOR inhibits ULK1 (*26*–*30*), AMPK controls ULK1 via a two-pronged mechanism, ensuring activation only under the appropriate cellular conditions (Fig. 4G and fig. S21). There are a number of physiological and pathological contexts in which this pathway is likely to play a critical role (*31*). Beyond the conserved nature of these signaling events and the role of some autophagy genes as tumor suppressors (*25*, *32*), AMPK is defective in a variety of human cancers bearing inactivating mutations in its upstream kinase LKB1. Thus, ULK1 may have a central role in the beneficial effects of the LKB1/AMPK pathway on tumor suppression or in treatment of metabolic disease, as observed here with metformin stimulation of ULK1 phosphorylation in liver and the profound defect in autophagy in AMPK-deficient livers. ULK1-dependent effects on mitochondrial homeostasis and cell survival may represent additional beneficial effects of metformin and other AMPK activators in overall organismal health and life span (*33*).

References and Notes

1. D. G. Hardie, *Nat. Rev. Mol. Cell Biol.* **8**, 774 (2007).
2. D. B. Shackelford, R. J. Shaw, *Nat. Rev. Cancer* **9**, 563 (2009).
3. R. J. Shaw *et al.*, *Science* **310**, 1642 (2005).
4. C. He, D. J. Klionsky, *Annu. Rev. Genet.* **43**, 67 (2009).
5. N. Mizushima, *Curr. Opin. Cell Biol.* **22**, 132 (2010).
6. E. Y. Chan, *Sci. Signal.* **2**, pe51 (2009).
7. Materials and methods are available as supporting material on *Science* Online.
8. D. M. Gwinn *et al.*, *Mol. Cell* **30**, 214 (2008).
9. C. Behrends, M. E. Sowa, S. P. Gygi, J. W. Harper, *Nature* **466**, 68 (2010).
10. D. G. Hardie, *Gastroenterology* **131**, 973 (2006).
11. E. Y. Chan, A. Longatti, N. C. McKnight, S. A. Tooze, *Mol. Cell. Biol.* **29**, 157 (2009).

12. B. E. Crute, K. Seefeld, J. Gamble, B. E. Kemp, L. A. Witters, *J. Biol. Chem.* **273**, 35347 (1998).
13. F. Andreelli *et al.*, *Endocrinology* **147**, 2432 (2006).
14. V. Kirkin, D. G. McEwan, I. Novak, I. Dikic, *Mol. Cell* **34**, 259 (2009).
15. S. Geisler *et al.*, *Nat. Cell Biol.* **12**, 119 (2010).
16. D. P. Narenda, L. A. Kane, D. N. Hauser, I. M. Fearnley, R. J. Youle, *Autophagy* **6**, 1 (2010).
17. M. Kundu *et al.*, *Blood* **112**, 1493 (2008).
18. S. Rodriguez-Enriquez, Y. Kai, E. Maldonado, R. T. Currin, J. J. Lemasters, *Autophagy* **5**, 1099 (2009).
19. M. Martinez-Vicente *et al.*, *Nat. Neurosci.* **13**, 567 (2010).
20. A. Melendez *et al.*, *Science* **301**, 1387 (2003).
21. C. Kang, Y. J. You, L. Avery, *Genes Dev.* **21**, 2161 (2007).
22. M. Hansen *et al.*, *PLoS Genet.* **4**, e24 (2008).
23. K. Jia *et al.*, *Proc. Natl. Acad. Sci. U.S.A.* **106**, 17534 (2009).
24. E. S. Hars *et al.*, *Autophagy* **3**, 93 (2007).
25. B. Levine, G. Kroemer, *Cell* **132**, 27 (2008).
26. C. H. Jung *et al.*, *Mol. Biol. Cell* **20**, 1992 (2009).
27. Y. Y. Chang, T. P. Neufeld, *Mol. Biol. Cell* **20**, 2004 (2009).
28. N. Hosokawa *et al.*, *Mol. Biol. Cell* **20**, 1981 (2009).
29. Y. Kamada *et al.*, *Mol. Cell. Biol.* **30**, 1049 (2010).
30. I. G. Ganley *et al.*, *J. Biol. Chem.* **284**, 12297 (2009).
31. D. Nakada, T. L. Saunders, S. J. Morrison, *Nature* **468**, 653 (2010).
32. R. Mathew, V. Karantza-Wadsworth, E. White, *Nat. Rev. Cancer* **7**, 961 (2007).
33. S. Fogarty, D. G. Hardie, *Biochim. Biophys. Acta* **1804**, 581 (2010).
34. We thank L. Gerken for mouse colony assistance, F. Esterman for confocal assistance, C. Chu for assistance in scoring LGG-1 assays, M. Wood at The Scripps Research Institute EM facility, X. Yang in the Beth Israel Deaconess Medical Center mass spectometry facility, R. Chitta from St. Jude's proteomic core, and K. Lamia for comments on the manuscript. D.F.E., D.M.G., and M.M.M. were supported through the T32 CMG training grant to the UCSD-Salk Biological Sciences Graduate Program. D.B.S. was funded by T32 CA009370 to the Salk Institute Center for Cancer Research. R.J.S. is funded by the NIH grants R01 DK080425 and 1P01CA120964, National Cancer Institute grant P30CA014195, an American Cancer Society Research Scholar Award, the American Diabetes Association Junior Faculty Award 1-08-JF-47, and a Howard Hughes Medical Institute Early Career Scientist Award. J.M.A. is supported by grants 5P30CA006516-43 and 1P01CA120964-01A. M.K. is funded by grant NHBLI K08, Burroughs Welcome Fund, and the American Lebanese Syrian Association. B.V. is supported by Agence Nationale de la Recherche (ANR). M.H. is an Ellison Medical Foundation New Scholar in Aging. We also thank the Leona M. and Harry B. Helmsley Charitable Trust for their generous support. Several of the authors (D.F.E., D.B.S., M.M.M, and R.J.S.) have filed a patent related to this work (U.S. patent application 61/325361).

Supporting Online Material

www.sciencemag.org/cgi/content/full/science.1196371/DC1
Materials and Methods
Figs. S1 to S21
References

11 August 2010; accepted 8 December 2010
Published online 23 December 2010;
10.1126/science.1196371

Effects of Experimental Seaweed Deposition on Lizard and Ant Predation in an Island Food Web

Jonah Piovia-Scott,* David A. Spiller, Thomas W. Schoener

The effect of environmental change on ecosystems is mediated by species interactions. Environmental change may remove or add species and shift life-history events, altering which species interact at a given time. However, environmental change may also reconfigure multispecies interactions when both species composition and phenology remain intact. In a Caribbean island system, a major manifestation of environmental change is seaweed deposition, which has been linked to eutrophication, overfishing, and hurricanes. Here, we show in a whole-island field experiment that without seaweed two predators—lizards and ants—had a substantially greater-than-additive effect on herbivory. When seaweed was added to mimic deposition by hurricanes, no interactive predator effect occurred. Thus environmental change can substantially restructure food-web interactions, complicating efforts to predict anthropogenic changes in ecosystem processes.

Global environmental change is expected to have a profound impact on the structure and function of ecological communities by changing interactions between their component species. Range shifts, extinctions, and species introductions change community composition, deleting some interactions and adding others (*1*, *2*). In addition, changes in the seasonal timing of migration and other life-history events can produce phenological mismatches, which can affect communities even when species composition is unchanged (*1*–*3*). The absence of alterations in species composition and phenology, however, does not necessarily mean that ecosystems will remain unaltered (*4*): Environmental change can also influence ecosystem processes by reconfiguring interactions in communities whose species lists remain intact (*5*–*9*).

Section of Evolution and Ecology and Center for Population Biology, One Shields Avenue, University of California Davis, Davis, CA 95616–8755, USA.

*To whom correspondence should be addressed. E-mail: jpioviascott@ucdavis.edu

An important aspect of global environmental change is the mobilization and transport of resources between ecosystems. Seaweed deposition in particular is likely to become a more common feature in shoreline ecosystems as anthropogenic effects (such as overfishing and eutrophication) facilitate a shift toward algae-dominated marine ecosystems (*10*). Furthermore, intense storms, which are associated with the deposition of large amounts of seaweed (*11*, *12*), have increased in frequency—a trend that is expected to continue with increasing global warming (*13*). Such pulsed inputs of external resources can increase prey availability, "subsidizing" in situ predators (*14*–*17*) and altering predator effects on lower trophic levels (*12*, *16*, *18*–*21*).

We used a whole-island field experiment in the Bahamas to probe how major seasonal pulses of seaweed deposition—mimicking what occurs in an active storm year (*22*)—influence the effects of multiple predators on herbivory in a terrestrial food web. Twelve small islands (one is shown in Fig. 1A), six with lizards and six naturally lizard-free, were used in the experiment. Seaweed was added or removed from islands in a crossed design; each combination of seaweed and lizard presence or absence was represented by three islands. Seaweed was manipulated in October and December of 2008, coinciding with that season when large storms are most likely to cause natural deposition events. On seaweed-addition islands, 0.4 to 1.4 kg/m^2 of seaweed was distributed patchily throughout each island, mimicking what occurs after a large storm (*22*). The removal treatment maintained seaweed at a level near zero, which is consistent with natural levels of about half of the islands before manipulation. Ant exclusions were established on branches of four (three in one case) *Conocarpus erectus* plants on each island; ants were excluded with a sticky resin, which lizards were able to bypass by crossing a narrow gap between wire mesh cones (Fig. 1B). Each of the four predator treatments in the experiment—(i) ants and lizards absent; (ii) ants present and lizards absent; (iii) ants absent and lizards present; and (iv) ants and lizards present—was represented by 12 branches in the absence of seaweed subsidy and 11 or 12 branches in the presence of seaweed subsidy.

Anolis sagrei was the only lizard species on the lizards-present islands. Previous experiments in this ecosystem demonstrated that *A. sagrei* reduced herbivory on *C. erectus* (*23*, *24*), one of the most common plants in shoreline habitats. Extrafloral nectaries on *C. erectus* foliage attract mutualistic ants, which can also decrease herbivory (*25*). The possibility that these two predators interactively affect lower trophic levels (*26*) had not been explored in previous studies.

Figure 1C shows a working model of the main food web components in our system. Seaweed deposits support an abundance of detritivores, which attract both ants and lizards (*12*). The most common herbivorous arthropods include Coleoptera, Lepidoptera, and Hemiptera (*12*). Previous studies in this system indicate that a shift in predator foraging behavior after two closely spaced pulses of seaweed is associated with increased herbivory on *C. erectus* (*12*), suggesting that the subsidies

Phosphorylation of ULK1 (hATG1) by AMP-Activated Protein Kinase Connects Energy Sensing to Mitophagy

Daniel F. Egan, David B. Shackelford, Maria M. Mihaylova, Sara Gelino, Rebecca A. Kohnz, William Mair, Debbie S. Vasquez, Aashish Joshi, Dana M. Gwinn, Rebecca Taylor, John M. Asara, James Fitzpatrick, Andrew Dillin, Benoit Viollet, Mondira Kundu, Malene Hansen and Reuben J. Shaw

Science **331** (6016), 456-461.
DOI: 10.1126/science.1196371originally published online December 23, 2010